VALIDATION OF THE CFD CODE USED FOR DETERMINATION OF AERODYNAMIC CHARACTERISTICS OF NON-STANDARD AGARD-B CALIBRATION MODEL

by

Nenad D. VIDANOVIĆ [a*], Boško P. RAŠUO [b], Dijana B. DAMLJANOVIĆ [c], Djordje S. VUKOVIĆ [c], and Dušan S. ĆURČIĆ [c]

[a] Faculty of Transport and Traffic Engineering, University of Belgrade, Belgrade, Serbia
[b] Faculty of Mechanical Engineering, University of Belgrade, Belgrade, Serbia
[c] Military Technical Institute, Belgrade, Serbia

Original scientific paper
DOI: 10.2298/TSCI130409104V

The application of CFD is often motivated by the limitations of measurement techniques, economic limitations, and complex model geometry or, as it is in this case, the unavailability of appropriate test model geometry. CFD was used to assess and evaluate scenario that cannot be investigated experimentally and was shown to be an efficient and economical option to experimental set-up. Because of that, there is a strong need for a validation procedure and assessment of the data obtained by numerical simulation. A combined experimental/numerical procedure is described for determination and estimation of subsonic and supersonic aerodynamic behaviour of an AGARD-B model with a non-standard nose configuration. Conducted numerical aerodynamic calculations needed to be satisfied via experimental tests so, the CFD code validation procedure required experimental data that characterize the distributions of measured aerodynamic forces and moments which act upon the test model. Validation of the CFD was achieved by performing the calculation for the model with the standard nose shape as well, and by comparing the results of the CFD calculations with available experimental data for the model with the standard nose configuration. Comparison demonstrated very good agreement between numerically and experimentally obtained results. It was concluded that the numerical prediction for the similar non-standard model configuration could be accepted as reliable and used to estimate the corrections needed when interpreting the available data. The effects of the different nose shape were found to be small and noticeable mainly in the pitching moment coefficient. This work also demonstrates the application of CFD for the purpose of proving a qualitative and quantitative prediction of the aerodynamics behaviour.

Key words: *experimental aerodynamics, wind tunnel validation, calibration model, CFD modeling, code calibration, aerodynamic coefficients*

Introduction

CFD has become a widely used tool for developing, supporting, optimizing, innovating, verifying and, especially here, for validating procedures. Verifying and validating represent

* Corresponding author; e-mail: n.vidanovic@sf.bg.ac.rs

forerun steps for the code calibration procedure. Verification procedure gives confirmation if the selected mathematical model is solved correctly by the CFD code and could be proved by comparing diverse turbulence models. Verification procedure was not conducted in this work, but credibly and widely used SST k-ω turbulence model was selected for qualitative/quantitative prediction of aerodynamics behaviour. It is useful to emphasis, as underlined in [1], that validation procedure is the practice of determining the domain in which a selected numerical model gives an accurate representation of the real problem, where the main goal is to quantify and qualify the accuracy of the numerical results through comparisons with available experimental data, and that the calibration procedure assesses the ability of a CFD code to predict global quantities of interest for specific engineering problems.

With respect to all above mentioned, wind tunnel experiment and CFD simulation of the flow past over a theoretical AGARD-B model must be conducted. After code calibration procedure, a validated numerical method could be used to evaluate the aerodynamic characteristics over a non-standard AGARD-B model with circular nose configuration.

Standard (calibration) wind tunnel models are important tools in calibrating both wind tunnel installations and numerical flow simulation algorithms. Mentioned AGARD series of standard models (AGARD-A, B, C, D, and E) is widely used in wind tunnel calibration measurements. There is an extensive database available with results from wind tunnel tests of these models in various experimental facilities worldwide, so that a comparison with results from the facility being calibrated is possible, [2]. Military Technical Institute in Belgrade (VTI) has used the AGARD-B and AGARD-C models of $D = 115.8$ mm body diameter in the initial calibration of its T-38 wind tunnel and continues to use them for periodical checkouts of the calibration of the facility. Results are compared primarily with those [3-7] from a very similar Canadian wind tunnel, and also with those from the compilation [8] which is a de-facto reference for the particular model type. The AGARD-B model that is used in VTI was produced by Boeing, USA, and, before being tested in VTI, had been used for a number of years in the NAE 5ft wind tunnel, the Romanian 1.2 × 1.2 m trisonic wind tunnel [9], and, previously, by Boeing. The results of the Boeing tests are cited in [8], but with a warning that the contour of the nose section of the model was different from the theoretical one, namely, being a body of rotation defined by a circular arc with a radius $r = 9.274$D where D is the model body diameter, instead of the nominal parabolic arc defined by the equation $r = (x/3)[1 - (1/9)(x/D)^2 + (1/54)(x/D)^3]$. Therefore, the results of this particular model cited in [8] were under a shadow of doubt and were not used in inter-facility comparison of VTI results. The nose section of the model has since been changed to the standard contour, so that the tests in VTI were performed with the correct configuration.

Recently, it was decided to estimate the effects of the error in the initial geometry of the model, so that necessary corrections could be made and results from [8] maybe used in inter-facility comparisons. The idea was to conduct CFD simulation of the circular-arc nose configuration of the AGARD-B model in order to determine the deviation of the aerodynamic characteristics of interest. Because of that, the correspondence between the correct parabolic-arc nose configuration test results and CFD calculations had to be achieved. So, the first step was to compare test data measurements with CFD calculations of the AGARD-B theoretical configuration. After determining the correspondent agreement between the computed and experimental results of an initial model configuration, CFD was used for further analysis of the circular-arc nose shape in a way that enabled obtaining relevant aerodynamic results. The T-38 trisonic blow-down pressurized wind tunnel in VTI was employed for experimental determination of the aerodynamic characteristics for the test model.

Wind tunnel testing

Wind tunnel facility

The T-38 test facility, presented by fig. 1(a), is a trisonic blow-down pressurized wind tunnel, placed in the VTI in Belgrade [10, 11]. Possible Reynolds numbers up to 110 million per meter, can be reached through a test process in this test facility [12]. Depending on appropriate Mach number, which can be selected from the range 0.2 to 4.0, and hence, depending on stagnation pressure, run times are in the range between 6 seconds and 60 seconds [12]. When T-38 operating in subsonic and supersonic test regimes, facility considering the use of test section with solid walls, while for transonic tests, wind tunnel configuration must be equipped with porous walls [11, 13]. With respect to the flow speed range, maintenance of configured Mach number can be achieved by means of a sidewall flaps, sidewall blow-off or by flexible nozzle. In the test section, stagnation pressure, which depends on selected Mach number, can be achieved and maintained in the range 1.1 bar to 15 bar, [13]. Sting configuration represents model support body in a 1.5 m × 1.5 m square test section, which is mounted on rolling and pitching mechanism, and enables aerodynamic angles adjusting in both mode, continuously and sequentially movement of a model during measurement process. Figure 1(b) presents AGARD-B model mounted on model support by sting body and placed in the test section of T-38.

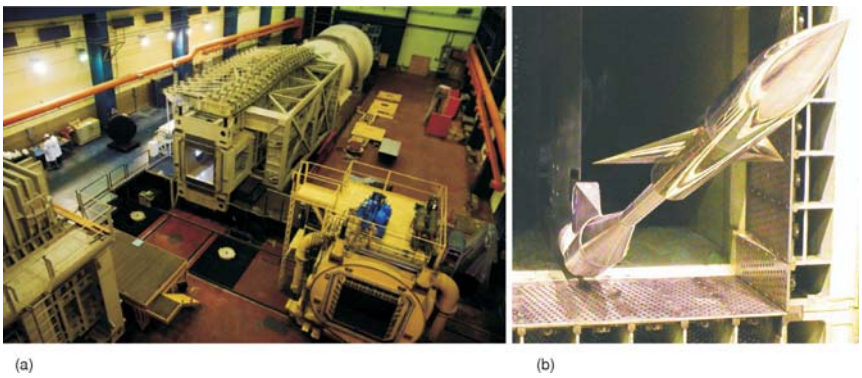

Figure 1. The T-38 test facility (a) with AGARD-B model placed in the test section (b)

Wind tunnel model

The AGARD calibration model B is a configuration consisting of a wing and body combination [5, 8, 9]. The wing is a delta in the form of an equilateral triangle with a span four times the body diameter and has a 4% thickness/chord ratio bi-convex section. The body is a cylindrical body of revolution with an ogive nose defined by two diverse curve types, parabolic one and circular one. Figure 2 is a representation of the model with the relevant dimensions given in terms of the body diameter *D*.

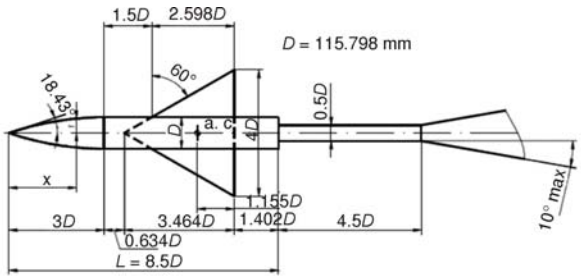

Figure 2. Basic dimensions of the AGARD-B test model

Table 1. Basic and reference model dimensions

Model length (L)	0.9843 m
Model diameter (D)	0.1158 m
Wing span (B)	0.4632 m
Model reference length, mean aerodynamic chord (L_{ref})	0.2674 m
Model reference length, wing span (B_{ref})	0.4632 m

Basic model dimensions of the AGARD-B standard model used in the T-38 wind tunnel facility (fig. 1) are given in tab. 1.

Standard *i. e*. theoretical AGARD-B model with parabolic nose configuration was used to provide force and moment data. Internal six-component strain gauge balance, which was used for data measuring, is described in the literature [3-7]. The sting was attached to the balance on the one side and with model base on the other side. Ratio between sting diameter and model base diameter was 0.5 and ratio between model base diameter and sting length was 5.2 (fig. 2). The angle of 7.9° was the conical evolution angle of sting into support. The reference point for force and moment calculation was located at 2.557D upstream of the model base or 1.155D distance upstream of the downstream edge of the wings, (fig. 2).

Instrumentation, data recording and reduction

This section briefly deals with instrumentation, which was used for divers measuring, data acquisition system and reduction procedure. The overview of instrumentation and procedures is presented in the following order:

– an absolute pressure transducer was used for stagnation pressure measuring and this transducer was pneumatically connected to a pitot probe and placed in the settling chamber of the wind tunnel,
– an piezoresistive differential pressure transducer was used for base pressure measuring,
– in subsonic speed range, difference between stagnation and static pressure was measured by a differential pressure transducer placed in the test section, and this transducer was pneumatically connected to the pitot probe and an orifice on sidewall,
– an absolute pressure transducer, used for supersonic measuring, was of the same range and of the same type, like aforementioned used for subsonic measuring,
– an resistance temperature detection probe, mounted in the settling chamber, was used for stagnation temperature measuring, and
– onto the movable mechanism mounted, the pitching angle measuring resolver was used.

Digitized data, collected by the data acquisition system, were sent through the network to a data processing computer. Sent data were stored on disk, prepared for later data reduction, which was performed using the T-38 application software package, developed in VTI. Wind axes system was used in data reduction and reduction procedure was performed in four stages:

– data acquisition system interfacing and signals normalization,
– flow parameters determination,
– model position determination, and
– aerodynamic coefficients determination.

The accuracies and the operating ranges of above cited transducers, performing procedures for calibration and acquisition processes, and other proper details about mentioned devices are presented in the literature [3-7].

Wind tunnel test results

Wind tunnel tests were performed for the purpose of checkout of the T-38 wind tunnel facility, with the standard AGARD-B model configuration (*i .e.* the one having a parabolic-arc nose ogive), at nominal Mach numbers 0.6 and 1.6, Angles of attack (AOA) in the interval –4 to +12 , and roll angle 0°, [5]. The obtained test results *vs*. corresponding CFD results are presented in comparative form in the section *Results and discussion*. Test results are given for model aerodynamic centre located a 2.557*D* distance upstream of the model base. Mega-Reynolds numbers for each Mach number, 6.42 for Ma = 0.596 and 9.97 for Ma = 1.602, are also given. Model reference length for Reynolds number calculation is the mean aerodynamic chord L_{ref}. Results from [3-7] were compared with those from the tests of the same model in a very similar Canadian wind tunnel and a excellent agreement was found (percent error is less than 1% of the largest measured values), so that they can be accepted with considerable confidence.

Computational fluid dynamics simulation

Numerical simulation of the flow plays a significant role for understanding the physical phenomena. The CFD modelling must be robust relating to changes and gradients of the physical properties of the fluid, which leads to qualitatively and quantitatively aerodynamics behaviour prediction. The current section investigates the use of CFD in the prediction of aerodynamic coefficients for both AGARD-B configurations. The flow solver used for this study was the FLUENT of ANSYS software. The viscous CFD simulations were used to calculate flowfield around the AGARD-B test models in subsonic and supersonic regimes. Computations were performed at 0.596 and 1.602 Mach numbers of interest at AOA –5° to 12°.

AGARD-B solid model, boundary conditions and computational mesh

The AGARD-B calibration models were modeled without a sting, for more accurate base drag component prediction and faster convergence. Two geometries were generated for the CFD studies, one with parabolic-arc and the other with circular-arc nose ogive configuration. Parametric AGARD-B configurations were modeled in the DESIGN MODELER environment of ANSYS.

The computational domain, with no hard boundaries around the model, was modeled to be a part of paraboloid with 15 model body lengths upstream from the tip of the model nose, 20 model body lengths downstream from the model base and with semi-axis of the paraboloid base with 25 models body lengths. Static temperature and static pressure were calculated with respect to their appropriate total values according to flowfield Mach number. The symmetry boundary condition for half configuration was selected because of the wind tunnel symmetry test conditions *i. e.* no-lateral-loads test conditions were performed. This boundary condition is also more effective in consumption of computational resources. All surfaces of the AGARD-B model were defined as a stationary no-slip adiabatic wall conditions.

The unstructured hybrid mesh was generated using the MESH (ANSYS ICEM CFD) environment of ANSYS software package. In most cases, mesh was automatically generated with respect to selected mesh growth rate of 1.08, but mentioned growth rate parameter was chosen to vary up to value of 1.20. Selection of appropriate growth rate parameter value, directly affects total grid size. The finest grid was defined with total cells number of 9841948 elements or 2636125 nodes which corresponds to growth rate parameter of 1.08. This density of the mesh was selected with respect to the sufficient amount of computer memory and convergence criteria of the calculated aerodynamic coefficients and residuals. It should be noted that a grid with the

total number of cells of about 7 million was fund to be sufficient to obtain a good agreement with test results and to ensure convergence of the calculated aerodynamic coefficients and residuals. A finer grids between 7 million and 10 million elements ensured a grid-independent solution. Selection of proper grid size, and hence, appropriate value of growth rate parameter, was influenced by changes and gradients of the physical properties of the fluid, based on Mach number and adequate AOA of interest.

The boundary layer was modeled with 20 layers and 1.2 growth rate and the height of the first cell was chosen to give y^+ value of about 1.0. The wall boundary layer resolution with y^+ being about 1.0 in the finest grid was in the domain of viscous sub-layer. The boundary layer was resolved with 2829360 elements or 1492197 nodes.

Numerical calculation

The steady-state (the results represent mean conditions), density-based type solver was used to compute the flowfield. The implicit formulation with Roe-FDS flux type was selected for solution method. The least square cell based for gradient and the second order upwind scheme for flow, turbulent kinetic energy and specific dissipation rate were selected for spatial discretization, [14]. Menter's [15-18] (shear-stress transport) SST k-ω turbulence model was selected for the numerical calculation of the flow in the computational domain. The SST model combines the k-ε and the k-ω models using a blending function. This SST model changes from the standard turbulence/frequency-based k-ω model in the near-wall region to a higher Reynolds number k-ε model in the far field. For the air flow prediction the Navier-Stokes equations have to be solved. The 3-D, time-dependent, Reynolds-Averaged Navier-Stokes equations are discretised using a cell-centered finite volume approach [19, 20]. The main control over the time-stepping scheme is the Courant number (CFL) which was defined to be automatically updated from 5 to 200 for both Mach numbers and all AOA. The fluid solver simultaneously solves the governing equations of continuity, momentum, and energy. The entire system of governing equations in conservation form [20], can be given by eq. (1):

$$\frac{\partial}{\partial t}\vec{\mathrm{U}} + \frac{\partial}{\partial x}\vec{\mathrm{F}} + \frac{\partial}{\partial y}\vec{\mathrm{G}} + \frac{\partial}{\partial z}\vec{\mathrm{H}} = 0 \tag{1}$$

where the column vectors $\vec{\mathrm{U}}$, $\vec{\mathrm{F}}$, $\vec{\mathrm{G}}$, and $\vec{\mathrm{H}}$ are defined as:

$$\vec{\mathrm{U}} = \begin{Bmatrix} \rho \\ \rho u \\ \rho v \\ \rho w \\ \rho E \end{Bmatrix}, \quad \vec{\mathrm{F}} = \begin{Bmatrix} \rho u \\ \rho u^2 + p - \tau_{xx} \\ \rho vu - \tau_{xy} \\ \rho wu - \tau_{xz} \\ \rho uE + pu - q_x - u\tau_{xx} - v\tau_{xy} - w\tau_{xz} \end{Bmatrix}$$

$$\vec{\mathrm{G}} = \begin{Bmatrix} \rho v \\ \rho uv - \tau_{yx} \\ \rho v^2 + p - \tau_{yy} \\ \rho wv - \tau_{yz} \\ \rho vE + pv - q_y - u\tau_{yx} - v\tau_{yy} - w\tau_{yz} \end{Bmatrix}, \quad \vec{\mathrm{H}} = \begin{Bmatrix} \rho w \\ \rho uw - \tau_{zx} \\ \rho vw - \tau_{zy} \\ \rho w^2 + p - \tau_{zz} \\ \rho wE + pw - q_z - u\tau_{zx} - v\tau_{zy} - w\tau_{zz} \end{Bmatrix}$$

The column vectors $\vec{F}$, $\vec{G}$, and $\vec{H}$ are called the flux terms and column vector $\vec{U}$ – is called the solution vector. Here ρ, E, and p are the density, total energy and pressure, and u, v, w are velocity components of the fluid, respectively. τ is the viscous stress tensor and $\vec{q}$ – the heat flux vector.

Numerical calculations were performed in parallel environment on Asus Workstation with two octa-core 2.00 GHz Intel Xeon E5-2650 processors and 64 GB RAM. The operating system addresses two logical cores for each physical core and can shares the workload between them. So, when we express physical cores in a "logical manner" for this configuration, we exactly deal with 32 logical cores which may be expressed with 32 processes. Total amount of 8 processes were allocated to each numerical calculation and each numerical calculation represents simulation per AOA. This configuration, with respect to earlier mentioned, enables employment up to three calculations in parallel mode, depending on memory consumption per calculation. Total memory usage per AOA was influenced by earlier determined grid size and could vary between 21 and 31 GB RAM. The convergence was depending on the Mach number and the AOA and was achieved approximately in about 1000-2000 iterations. Total CPU time of about 56 CPU hours describes the total CPU time used by eight processes per AOA and this does not include any wait time for load imbalances or for communications. The simulations were interrupted when the difference between aerodynamic coefficients were less than 1% during 100 previous iterations.

Results and discussion

The test results of AGARD-B theoretical calibration model, with the standard parabolic nose ogive configuration, are compared with the results obtained from the CFD simulations that were conducted for both model configurations, one with parabolic and the other with circular nose ogive. The comparative results are presented in the form of graphs in figs. 6, 7 and 8, which show C_m, C_L, and C_D in relation to the angle of attack in the wind axes system. It can be seen that there is no significant differences between CFD-simulated circular and experimentally obtained results for theoretical model which is in accordance with reference [8]. However, the differences are presented and certain domains need to be discussed.

Pressure distribution on lower and upper AGARD-B model surfaces in comparative form for both Mach numbers and three specific AOA (–4°, 0°, and 11°) are presented in following figures (figs. 3, 4, and 5).

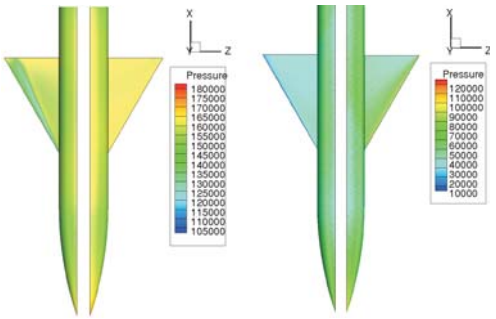

Figure 3. Pressure distribution on lower and upper AGARD-B model surfaces for Ma = 0.596 (left) and Ma = 1.602 (right) at –4° AOA

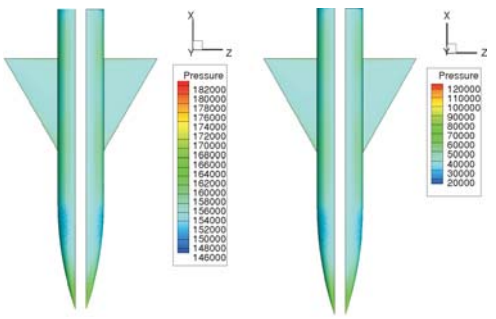

Figure 4. Pressure distribution on lower and upper AGARD-B model surfaces for Ma = 0.596 (left) and Ma = 1.602 (right) at 0° AOA

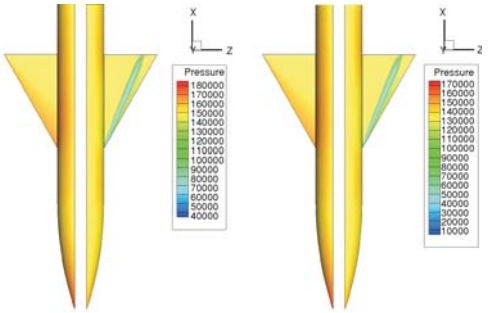

Figure 5. Pressure distribution on lower and upper AGARD-B model surfaces for Ma = 0.596 (left) and Ma = 1.602 (right) at 11° AOA

The first two graphs in fig. 6 represent C_m *vs.* AOA for Ma = 0.596 and Ma = 1.602. It can be seen that simulated values of C_m are, for both model configurations, and the case of Ma = = 0.596, somewhat lower at higher angles of attack than experimental ones. Noticeable discrepancies occur for AOAs greater than 4°. For the Ma = 1.602 case, there are major differences between the simulated results for the parabolic-arc and circular-arc model noses. The results for the parabolic-arc nose configuration being much closer to the experimental ones. At both Mach numbers, the differences in C_m are more prominent in the region of AOA greater than 4°.

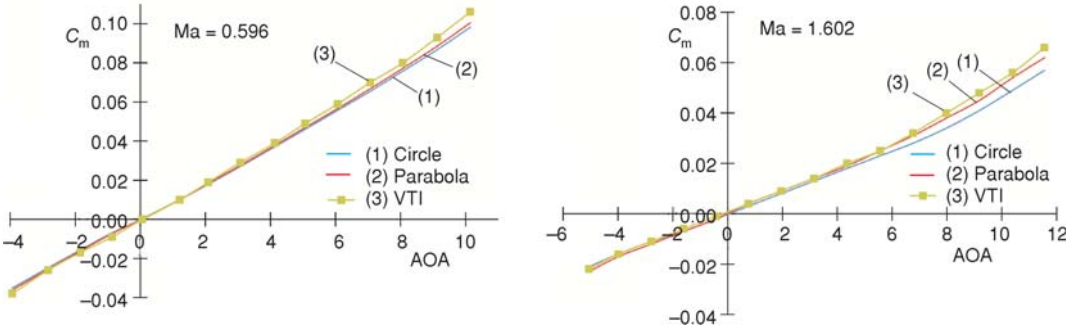

Figure 6. Experimental *vs.* CFD moment coefficient curves for Ma = 0.596 (left) and Ma = 1.602 (right)

The two graphs in fig. 7 represent C_L *vs.* AOA for Ma = 0.596 and Ma = 1.602. C_L graph for Ma = 0.596 case show no noticeable discrepancies between the experimental and simulated lift curves. On the other hand, noticeable discrepancies occur, for the Ma = 1.602 case, between the CFD curves and the experimental curve in the region of negative angles of attack, but an excellent agreement (percent error is less than 1% over all AOA domain) exist between

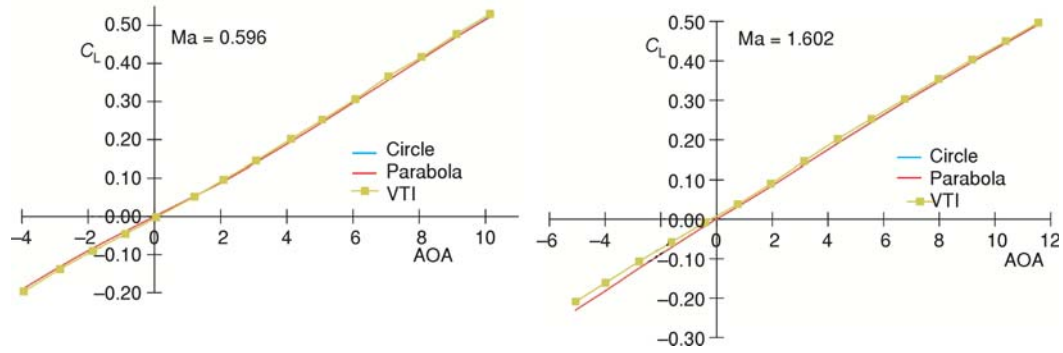

Figure 7. Experimental *vs.* CFD lift coefficient curves for Ma = 0.596 (left) and Ma = 1.602 (right)

the CFD curves. As the test results are not symmetrical with respect to 0º AOA (while they should be, for a symmetrical model), the discrepancy between the simulation and the experiment can be attributed to an experimental error, possibly caused by a non-linear behaviour of the force balance used in the test that was not accounted for in the calibration matrix. Another possible error sources in force measurements can be a slight asymmetry of the model or model dynamic motion, mechanical and structural balance design, influence of strain gages to flexures, deterioration of strain gages, attachment of the balance to the sting and to the model or attachment of the sting to the support system or influence of the angles of the support system. One can conclude that there is no significant difference between the C_L curves for any of the two nose configurations and the experimental results.

Finally, the two graphs in fig. 8 depict C_D *vs*. AOA for Ma = 0.596 and Ma = 1.602. It can be noted that there is an excellent agreement between all curves for Ma = 0.596 for all AOA. For the Ma = 1.602 case, there is an percent error between 0.3% and 3% at positive AOA between the experimental and the simulated results for the parabolic-arc nose configuration, and error between 3% and 5% for the simulated results for the circular-arc nose configuration. For the parabolic-arc nose configuration at negative AOA the experimental results deviate slightly (between 3% and 5%) from the simulated ones, which can be caused by the above-mentioned experimental error in the measurement of normal force, but for circular-arc nose configuration difference is between 0.3% and 3%.

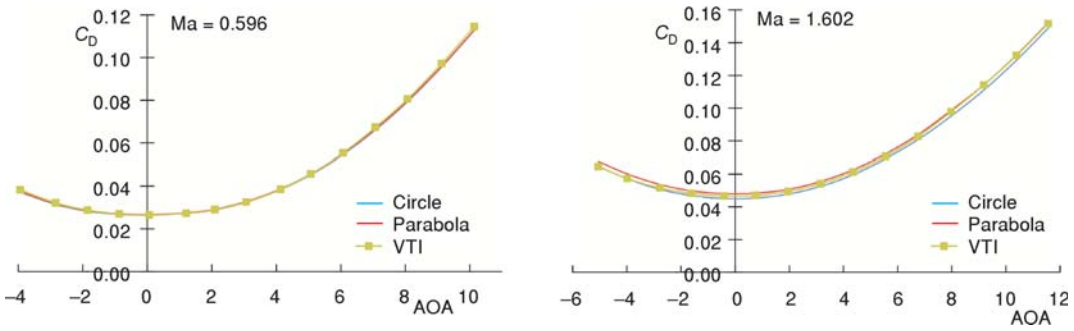

Figure 8. Experimental *vs.* CFD drag coefficient curves for Ma = 0.596 (left) and Ma = 1.602 (right)

All presented results suggest that CFD simulations of the subsonic and supersonic behaviour of the two configurations of the AGARD-B model are, mostly, in very good agreement with the experimental results (percent error is less than 5% of the largest simulated cases). This is the very reason why CFD simulation is used here for differences evaluation between model with parabolic and circular nose ogive configuration for which there is a lack of available experimental results and very limited recommendations. That means that conducted simulations with applied SST k-ω turbulence model can give satisfactory predictions for aerodynamic behaviour and can yield encouraging results in subsonic and supersonic external flow cases and represents very acceptable numeric for validation procedure. So, when we deal with well validated SST k-ω turbulence model, we actually use a reliable numeric, and hence, no verification procedure is necessary.

Generally speaking, in accordance with the conducted investigation, it can be assumed that aerodynamic behavior in subsonic and supersonic flows for these two model configurations

can be credibly numerically predicted and that the calibrated procedure for this similar cases were very well done.

Conclusions

Calculations show that the applied turbulent model qualitatively predicts the main features of the aerodynamics behaviour. This means that trends of numerically-simulated curves are in excellent agreement with trends of experimentally-obtained ones. Furthermore, trends between numerically-obtained curves for two similar nose configurations are in excellent agreement, too. Therefore, the behaviour of the circular-arc-nose configuration can be deduced from the simulation, concluding that the main effect of the change of the nose shape is reflected in a change of the pitching moment coefficient, while the effect of the nose shape is smaller on the drag coefficient and practically negligible on the lift coefficient.

It can be concluded that the experimentally validated code for subsonic and supersonic flows can be used to predict the results, for the same flows, of the aerodynamic coefficients of the model with a different, but similar geometry. Transonic behavior requires deeper analyzing and successive simulations and it may be a part of a future investigation. Numerical flow simulation around AGARD-B mounted on the sting may be a part of a future investigation too, especially for the case of possible influence on base pressure distribution.

It is very important to emphasis that CFD can be useful tool for assessment procedure of diverse geometry types that often cannot be sufficiently covered by measurements. Nevertheless, wind tunnel measurements of the flowfields are necessary to validate and calibrate such simulations and to provide adequate boundary conditions. Finally, once the code is well validated, one can rely on the CFD process for further aerodynamic investigation. Thus, CFD is a capable tool for more than preliminary investigations, but never separated from the experiments.

Nomenclature

C_D – drag coefficient, [–]
C_L – lift coefficient, [–]
C_m – moment coefficient, [–]
D – model body diameter, [m]
E – total energy, [J]
k – turbulence kinetic energy, [m^2s^{-2}]
Ma – Mach number (= U/c), [–]
p – pressure, [Pa]
q – heat flux, [Wm^{-2}]
Re – Reynolds number (= UL_{ref}/ν), [–]
r – curve radius, [m]
u – x velocity component, [ms^{-1}]
v – y velocity component, [ms^{-1}]
w – z velocity component, [ms^{-1}]
y^+ – dimensionless length parameter, [–]

Greek symbols

ε – turbulent dissipation rate, [m^2s^{-3}]
ρ – density, [kgm^{-3}]
τ – viscous stress, [Pa]
ω – specific dissipation rate, [s^{-1}]

Acronyms

AGARD – advisory group for aerospace research and development
AOA – angle of attack
CFD – computational fluid mechanics
SST – shear stress transport
VTI – Vojnotehnički Institut (Military Technical Institute)
FDS – flux-difference splitting
CFL – courant-Friedrichs-Lewy (= $\Delta t \Sigma u x_i / \Delta x_i \leq CFL_{max}$; $i = 1, n$)

References

[1] Colombo, E., *et al.*, A Methodology for Qualifying Industrial CFD: The Q3 Approach and the Role of a Protocol, *Computers & Fluids, 54* (2012), Jan., pp. 56-66
[2] Rasuo, B., Scaling between Wind Tunnels-Results Accuracy in Two-Dimensional Testing, *Transactions of the Japan Society for Aeronautical & Space Sciences, 55* (2012), 2, pp. 109-115

[3] Damljanović, D., Investigation of Flow Quality Parameters in the 3D Test Section of the T-38 Trisonic Wind Tunnel (in Serbian), M. Sc. thesis, Faculty of Mechanical Engineering, University of Belgrade, Belgrade, 2010
[4] Damljanović, D., Rašuo, B., Testing of Calibration Models in Order to Certify the Overall Reliability of the Trisonic Blowdown Wind Tunnel of VTI, *FME Transactions, 38* (2010), 4, pp. 167-172
[5] Damljanović, D., *et al.*, Testing of AGARD-B Calibration Model in the T-38 Windtunnel, *Scientific Technical Review, 56* (2006), 2, pp. 52-62
[6] Damljanović, D., *et al.*, An Evaluation of the Overall T-38 Wind Tunnel Data Quality in Testing of a Calibration Model, *Proceedings*, 30th AIAA Applied Aerodynamics Conference, New Orleans, Louisiana, 2012
[7] Damljanović, D., *et al*., The T-38 Wind Tunnel Data Quality Assurance Based on Testing of a Standard Model, *AIAA Journal of Aircraft*, *50* (2013), 4, pp. 1141-1149
[8] Hills, R., A Review of Measurement on AGARD Calibration Models, Report No. 64, Aircraft Research Association, Bedford, England, 1961
[9] Isakovic, J., *et al*., Testing of the AGARD B/C, ONERA and SDM Calibration Models in the T-38 1.5m x 1.5m Trisonic Wind Tunnel, *Proceedings*, 19th ICAS Congress, Anaheim, Cal., USA, 1994, pp. 1-9
[10] Elfstrom, G. M., Medved, B., The Yugoslav 1.5 m Trisonic Blowdown Wind Tunnel, AIAA Paper 86-0746-CP, 1986
[11] Rasuo, B., Two-Dimensional Transonic Wind Tunnel Wall Interference, Technical University of Budapest, Budapest, 2003
[12] Rasuo, B., The influence of Reynolds and Mach Numbers on Two-Dimensional Wind-Tunnel Testing: An Experience, *The Aeronautical Journal, 115* (2011), 1166, pp. 249-254
[13] Rasuo, B., On Boundary Layer Control in Two-Dimensional Transonic Wind Tunnel Testing, *Proceedings*, (Eds. G. E. A. Meier, K. R. Sreenivasan, H.-J. Heinemann), IUTAM Symposium on One Hundred Years of Boundary Layer Research, Berlin, Germany, 2006, pp. 473-482
[14] ***, ANSYS Inc., Theory Guide, ANSYS FLUENT 14.0, 2009
[15] Menter, F. R., Performance of Popular Turbulence Models for Attached and Separated Adverse Pressure Gradient Flow, *AIAA J., 30* (1992), 8, pp. 2066-2072
[16] Menter, F. R., Improved Two-equation k-ω Turbulence Models for Aerodynamic Flows, NASA Technical Memorandum TM-103975, NASA Ames, Cal., 1992
[17] Menter, F., Two-Equation Eddy-Viscosity Turbulence Model for Engineering Applications, *AIAA J., 32* (1994), 8, pp. 1598-1605
[18] Menter, F., Eddy-Viscosity Transport Equations and their Relation to the k-ε Model, *Trans. ASME, J. Fluids Eng., 119* (1997), 4, pp. 876-884
[19] Versteeg, H. K., Malalasekera, W., *An Introduction to Computational Fluid Dynamics*, 2nd ed., Pearson Education Limited, Harlow, England, 2007
[20] Anderson, D. J., *Computational Fluid Dynamics,* McGraw-Hill Inc., New York, N. Y., 1995

Paper submitted: April 9, 2013
Paper revised: May 17, 2013
Paper accepted: July 16, 2013